Inorg. Chem. **2004**, *43*, 385–391

Molten Flux Synthesis of an Analogous Series of Layered Alkali Samarium Selenogermanate Compounds

Benjamin R. Martin and Peter K. Dorhout*

Department of Chemistry, Colorado State University, Fort Collins, Colorado 80523

Received June 24, 2003

In this work, we used the molten chalcogenide flux synthetic method to form an analogous series of alkali samarium selenogermanates, with the general formula $ASmGeSe_4$ (A = K, Rb, Cs). Using a constant reactant stoichiometry, we relate the monoclinic $KLaGeSe_4$ structure type to the orthorhombic $CsSmGeS_4$ structure type. $KSmGeSe_4$ [in space group $P2_1$ with cell parameters $a = 6.774(1)$ Å, $b = 6.994(1)$ Å, $c = 8.960(2)$ Å, $\beta = 108.225(3)°$, and $V = 403.2(1)$ Å^3 ($Z = 2$)], $RbSmGeSe_4$ [in space group $P2_12_12_1$ with cell parameters $a = 6.7347(8)$ Å, $b = 7.0185(9)$ Å, $c = 17.723(2)$ Å, and $V = 837.7(2)$ Å^3 ($Z = 4$)], and $CsSmGeSe_4$ [in space group $P2_12_12_1$ with cell parameters $a = 6.707(2)$ Å, $b = 7.067(2)$ Å, $c = 18.334(6)$ Å, and $V = 869.1(5)$ Å^3 ($Z = 4$)] were formed under identical synthetic conditions by changing the identity of the alkali ion from K to Rb or Cs, respectively. Additionally, with the substitution of sodium into the reaction, a triclinic structure with the approximate formula $NaSmGeSe_4$ was found with the cell parameters $a = 6.897(2)$ Å, $b = 9.919(2)$ Å, $c = 11.183(2)$ Å, $\alpha = 84.067(4)°$, $\beta = 88.105(4)°$, $\gamma = 73.999(4)°$, and $V = 731.5(3)$ Å^3. In addition to single-crystal diffraction, Raman and diffuse reflectance UV–visible spectroscopic measurements have been used to characterize these compounds.

Introduction

The inclusion of rare earth (RE) metals in chalcogenide frameworks can result in new materials with interesting electrical,[1] magnetic,[2] and optical[3,4] properties. Systematic studies of the properties of these materials would benefit from the development of series of analogous materials, but unfortunately such systems are seldom found in solid-state compounds. We report here the synthesis of and structural relationships between three quaternary RE chalcogenide phases, including structures related to previously published sets of quaternary RE chalcogenides and a previously unknown triclinic phase.

The synthesis of RE chalcogenides has traditionally been undertaken through the reaction of rare earth oxides or metals with a molten or vaporous chalcogen source in high-temperature environments.[5] "Soft" synthetic methods utilizing lower temperature conditions, such as hydrothermal or flux syntheses, can allow access to thermodynamically metastable phases. Flux synthesis of RE chalcogenides via an alkali polychalcogenide flux has been shown to be extremely versatile and has resulted in the discovery of many new structures, some of which cannot be prepared by direct combination of the elements.[6]

The incorporation of main-group and alkali cations into the RE chalcogen frameworks allows the formation of many new, interesting RE-containing structures. These quaternary structures can be understood as being composed of building blocks formed from main-group−chalcogen polyhedra ($GeSe_4$ tetrahedra, for example), linked through RE polyhedra, and charge-balanced with alkali cations. The types of selenogermanate units that can be expected in quaternary chalcogenides can be deduced from ternary alkali selenogermanates. The most common building blocks observed in these materials are $GeSe_4$ tetrahedra, found in many ternary alkali selenogermanates, for example, Na_4GeSe_4.[7] More complex

* Author to whom correspondence should be addressed: fax 970-491-1801; e-mail pkd@LAMAR.colostate.edu.

(1) Mitchell, K.; Haynes, C. L.; McFarland, A. D.; Van Duyne, R. P.; Ibers, J. A. *Inorg. Chem.* **2002**, *41*, 1199−1204.
(2) Huang, F. Q.; Ibers, J. A. *J. Solid State Chem.* **2001**, *158*, 299−306.
(3) Kumta, P. N.; Risbud, S. H., *J. Mater. Sci.* **1994**, *29*, 1135−1158.
(4) Klocek, P., Ed. Window and Dome Technologies and Materials II. *Proc. SPIE* **1990**, *1326*.
(5) Guitard, M.; Flahaut, J. *Synthesis of Lanthanide and Actinide Compounds*; Meyer, G., Morss, L. R., Eds.; Kluwer: Boston, MA, 1991; pp 321−347.
(6) Kanatzidis, M. G.; Sutorik, A. C. *Prog. Inorg. Chem.***1995**, *43*, 151−265
(7) Klepp, K. O. *Z. Naturforsch. B: Anorg. Chem., Org. Chem.* **1985**, *40B*, 878−882.

10.1021/ic034724y CCC: $27.50
Published on Web 12/09/2003

units include the adamantane-like Ge_4Se_{10} unit in $K_4Ge_4Se_{10}$,[8] as well as structures containing Ge−Ge bonds such as the ethane-like Ge_2Se_6 unit in $K_6Ge_2Se_6$.[9] It is reasonable to expect that with the right packing conditions these complex building blocks should be observed. Such units will alter the vibrational modes available to the structure and could result in interesting phase transitions under appropriate conditions.[10]

The search through quaternary phase space for new RE chalcogenides can be a daunting task, but targeting expected stoichiometries based upon known ternary selenogermanates can narrow the search. This model has been used to predict the stoichiometries of new quaternary RE selenides by employing selenophosphate polyhedra found in ternary alkali structures as building blocks for more complex structures.[11,12]

Preliminary phase-space explorations in quaternary A-Sm-Ge-Se (A = K, Rb, Cs) systems have revealed that layered structures containing tetrahedral $GeSe_4$ will form from all of the alkali metals in the series. In this paper, we show how the layered orthorhombic $CsSmGeSe_4$ and $RbSmGeSe_4$ structures (isostructural with $CsSmGeS_4$[13]) and the monoclinic $KSmGeSe_4$ structure (isostructural with $KLaGeSe_4$[14]) can be formed under nearly identical reaction conditions, simply by changing the alkali metal identity in the alkali selenide flux. A new triclinic unit cell was discovered for a compound with the approximate formula $NaSmGeSe_4$ (formula derived through electron microprobe analysis spectroscopy). Although the structure types presented here are isostructural with previously published compounds, this paper represents the first systematic study of the structural effects of alkali metal substitution in these quaternary structures without other complicating factors, like lanthanide substitution, or alternate synthetic methods.

Experimental Section

Synthesis. The following reactants were used as received and stored in an inert atmosphere glovebox: Sm (99.9%, Cerac), Ge (99.999%, Cerac), and Se (99.999%, Johnson-Mathey). Na_2Se_2, K_2Se_2, Rb_2Se_3, and Cs_2Se_2 were made from stoichiometric combination of the elements in liquid ammonia as described previously.[15,16] Reactants were loaded into fused silica ampules inside an inert atmosphere glovebox. The ampules were flame-sealed under vacuum and placed in a temperature-controlled furnace. The furnace was ramped to 725 °C at a rate of 35 °C/h, and the temperature was held constant at 725 °C for 150 h. The furnace was then slowly cooled to ambient temperature at a rate of 4 °C/h. After the reaction products cooled, the ampules were opened in an inert atmosphere glovebox, and the solid product was soaked in *N*,*N*-dimethylformamide (DMF) for 6 h in order to dissolve and wash away any remaining flux and loosen the product crystals. Although the quaternary products were stable in air for a period of days, the inert atmosphere prevented the precipitation of elemental selenium resulting from decomposition reactions of binary and ternary species during the washing process.

$KSmGeSe_4$, **I**, was synthesized by combining 75.8 mg of Sm (0.504 mmol), 73.8 mg of Ge (1.02 mmol), 159.7 mg of Se (2.02 mmol), and 80.7 mg of K_2Se_2 (0.342 mmol). After treatment with DMF, orange plates of $KSmGeSe_4$ were observed (approximately 95% of the solid product after DMF treatment), along with orange hemispheres of amorphous potassium selenogermanate (identified by electron microprobe analysis). Energy-dispersive X-ray analysis of **I** yielded atomic ratios 0.15 K, 0.15 Sm, 0.15 Ge, 0.55 Se (surface contamination limited the accuracy of these data to ±5%).

$RbSmGeSe_4$, **II**, was synthesized by combining 72.6 mg of Sm (0.483 mmol), 70.3 mg of Ge (0.968 mmol), 127.6 mg of Se (1.62 mmol), and 131.5 mg of Rb_2Se_3 (0.322 mmol). After treatment with DMF, orange plates of $RbSmGeSe_4$ were observed (approximately 75% of the solid product after DMF treatment), along with orange hemispheres of amorphous rubidium selenogermanate (identified by electron microprobe analysis). Energy-dispersive X-ray analysis of **II** yielded atomic ratios 0.15 Rb, 0.15 Sm, 0.15 Ge, 0.55 Se (surface contamination limited the accuracy of these data to ±5%).

$CsSmGeSe_4$, **III**, was synthesized by combining 75.4 mg of Sm (0.501 mmol), 72.8 mg of Ge (1.00 mmol), 164.5 mg of Se (2.08 mmol), and 144.5 mg of Cs_2Se_2 (0.341 mmol). After treatment with DMF, orange plates of $CsSmGeSe_4$ were observed (approximately 95% of the solid product after DMF treatment), along with orange hemispheres of amorphous cesium selenogermanate (identified by electron microprobe analysis). Energy-dispersive X-ray analysis of **III** yielded atomic ratios 0.15 Cs, 0.15 Sm, 0.15 Ge, 0.55 Se (surface contamination limited the accuracy of these data to ±5%).

$NaSmGeSe_4$ (approximate formula), **IV**, was synthesized by combining 39.7 mg of Sm (0.264 mmol), 57.3 mg of Ge (0.789 mmol), 83.6 mg of Se (1.06 mmol), and 26.9 mg of Na_2Se_2 (0.132 mmol). After treatment with DMF, a small number of orange-red plates of **IV** were observed (approximately 1% of the solid product after DMF treatment), along with elemental selenium, red-orange hexagonal plates of $NaSmSe_2$, orange hemispheres and yellow plates of sodium selenogermanates (identified by electron microprobe analysis), and $GeSe_2$. Energy-dispersive X-ray analysis of **IV** yielded atomic ratios 0.15 Na, 0.15 Sm, 0.15 Ge, 0.55 Se (surface contamination limited the accuracy of these data to ±5%). These values were used to calculate the approximate formula.

Physical Measurements. Single-Crystal X-ray Diffraction. Intensity data sets for compounds **I**−**III** were collected on a Bruker Smart CCD diffractometer. These data were integrated with SAINT,[17] a SADABS correction was applied,[18] and the structures were solved by direct methods with SHELXTL.[19] Selected crystallographic data and collection parameters for the structures are reported in Table 1.

Raman Spectroscopy. The bulk solid-state Raman spectra of compounds **I**−**III** were collected on a Nicolet Magna-IR 760 spectrometer with a FT-Raman Module attachment by use of a Nd:YAG excitation laser (1064 nm).

(8) Eisenmann, B.; Hansa, J. *Z. Kristallogr.* **1993**, *206*, 101−102.
(9) Eismann, B.; Kieselbach, E.; Schaefer, H.; Schrod, H. *Z. Anorg. Allg. Chem.* **1984**, *516*, 49−54.
(10) Burris, J. L.; Orgzall, I.; Evenson, C. R.; Dorhout, P. K.; Hocheimer, H. D. *J. Phys. Chem. Solids* **2002**, *63*, 597−603.
(11) Evenson, C. R.; Dorhout, P. K. *Inorg. Chem.* **2001**, *40*, 2875−2883.
(12) Evenson, C. R.; Dorhout, P. K., *Inorg. Chem.* **2001**, *40*, 2884−2891.
(13) Bucher, C. K.; Hwu, S.-J. *Inorg. Chem.* **1994**, *33*, 5831−5835.
(14) Wu, P.; Ibers, J. A. *J. Solid State Chem.* **1993**, *107*, 347−355.
(15) Liao, J.-H.; Kanatzidis, M. G. *Inorg. Chem.* **1992**, *31*, 431−439.
(16) Schewe-Miller, I. Metallreiche hauptgruppenmetall-Chalkogenverbindungen: Synthese, Strukturen and Eigenschaften. Ph.D. Thesis, Max-Planck-Institut fur Festkorperforschung, Stuttgart, Germany, 1990.
(17) *SAINT; Data processing software for the SMART system*; Bruker Analytical X-ray Instruments, Inc.; Madison, WI, 1995.
(18) Sheldrick, G. M. *SADABS*; University of Gottingen: Gottingen, Germany, 1997.
(19) *SHELXTL 5.1*; Bruker AXS Inc.: Madison, WI, 1998.

Table 1. Selected Crystallographic Data for $ASmGeSe_4$ Structures

	$KSmGeSe_4$ **I**	$RbSmGeSe_4$ **II**	$CsSmGeSe_4$ **III**
space group	$P2_1$ (4)	$P2_12_12_1$ (19)	$P2_12_12_1$ (19)
formula weight	577.88	624.25	671.69
a, Å	6.774(1)	6.7347(8)	6.707(2)
b, Å	6.994(1)	7.0185(9)	7.067(2)
c, Å	8.960(2)	17.723(2)	18.334(6)
β, deg	108.225(3)	90	90
Z	2	4	4
V, Å^3	403.2(1)	837.7(2)	869.1(5)
ρ, calc, g/cm^3	4.760	4.950	5.134
radiation wavelength, Å	0.710 73	0.710 73	0.710 73
linear abs. coeff, mm^{-1}	29.398	33.577	30.929
collection temp, K	298	298	298
absolute structure parameter	0.51(9)	0.51(8)	0.06(6)
R1[a] ($I > 2\sigma$)	0.0414	0.0336	0.0335
wR2[b] ($I > 2\sigma$)	0.0925	0.0608	0.0584

[a] $R1 = \Sigma||F_o| - |F_c||/\Sigma|F_o|$. [b] $wR2 = [\Sigma[w(F_o^2 - F_c^2)^2]/\Sigma[w(F_o^2)^2]]^{1/2}$.

UV−Visible Spectroscopy. Diffuse reflectance measurements were taken on a Varian Cary 500 Scan UV−vis−NIR spectrophotometer equipped with a Praying Mantis accessory. A polyTeflon standard was used as a reference. The Kubelka−Munk function was applied to obtain band-gap information.[20−22]

Results and Discussion

$KSmGeSe_4$, I. A single crystal of $KSmGeSe_4$, **I**, was selected, 2558 (1153 independent) reflections were collected, and an absorption correction was applied ($R_{int} = 0.0575$). Data were collected within a θ range of 3.17∠23.24° to a completeness of 99.8% with a data index range of $-7 \le h \le 7$, $-7 \le k \le 7$, $-9 \le l \le 9$. The structure was solved in $P2_1$ by direct methods with final electron density residuals of 2.33 and −1.60 e Å^{-3}, and all atoms were refined anisotropically on F^2 for 65 variables.[19] Fractional coordinates and isotropic displacement parameters for $KSmGeSe_4$ can be found in the Supporting Information.

$KSmGeSe_4$ is isostructural with $KLaGeSe_4$,[14] first reported by Wu and Ibers, but it is still interesting in the context of this series of structures because the $KLaGeSe_4$ structure type had not been directly linked to other quaternary structures. Figure 1a depicts **I** as viewed along the *a*-axis, and Figure 2a depicts the $SmGeSe_4$ layer along the *c*-axis. The coordination environments around Sm and Ge are visible as anisotropic displacement ellipsoids in Figure 3. **I** consists of a layered structure of corner- and edge-sharing monocapped trigonal-prismatic $SmSe_7$ polyhedra sharing corners and edges with $GeSe_4$ tetrahedra. The potassium cations occupy the interlayer sites and charge-balance the structure. Close examination of the structure reveals that the $SmSe_7$ polyhedra form edge-sharing chains along the *b* crystallographic direction, and these chains are linked together through shared corners via the capping ligands. The Se atoms involved with edge-shared $SmSe_7$ polyhedra are also corner-shared with $GeSe_4$ tetrahedra, and the Se atoms involved with corner-shared $SmSe_7$ polyhedra are edge-shared with $GeSe_4$ tetrahedra. Other detailed structural descriptions have been noted previously[14] and will not be repeated here.

I was modeled as a racemic twin with an absolute structure parameter of 0.51(9). Attempts were made to model **I** in a centrosymmetric space group, but in this structure, Sm is not in a symmetric environment, and centrosymmetric models fail (without introduction of a disorder model that effectively simulates the lower symmetry space group assignment). The

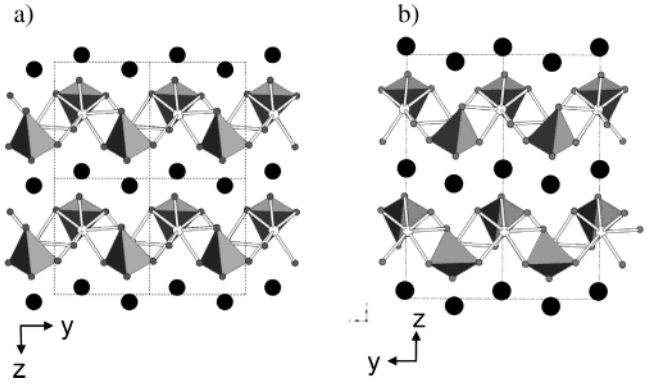

Figure 1. $ASmGeSe_4$ compounds viewed parallel to the $SmGeSe_4$ layers. Dotted lines indicate unit cell boundaries in each case. $GeSe_4$ tetrahedra are drawn as shaded solids, and the $SmSe_n$ environments are drawn as ball-and-stick models. In both structures, Sm is unshaded and Se is lightly shaded. (a) $KSmGeSe_4$ **I** viewed along *a*; K sites are shaded black. (b) $RbSmGeSe_4$ **II** viewed along *a*; Rb sites are shaded black.

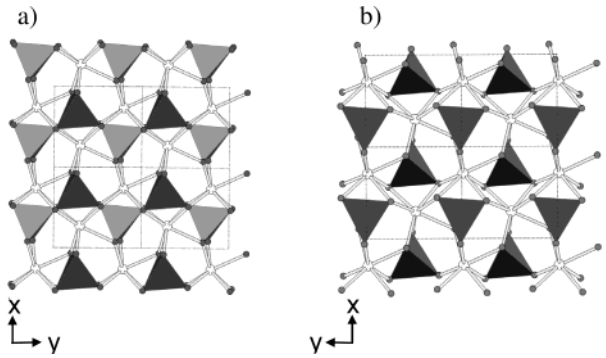

Figure 2. $ASmGeSe_4$ compounds viewed perpendicular to the $SmGeSe_4$ layers. Dotted lines indicate unit cell boundaries in each case. Alkali metal sites have been omitted for clarity. $GeSe_4$ tetrahedra are drawn as shaded solids, and the $SmSe_n$ environments are drawn as ball-and-stick models. In both structures, Sm is unshaded and Se is lightly shaded. (a) $KSmGeSe_4$ **I** viewed along *c*. (b) $RbSmGeSe_4$ **II** viewed along *c*.

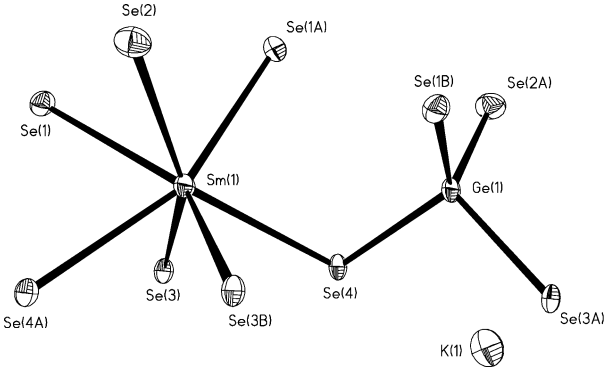

Figure 3. Thermal ellipsoid plot of $KSmGeSe_4$ **I**, showing anisotropic displacement ellipsoids at 50% probability.

(20) McCarthy, T. J.; Tanzer, T. A.; Kanatzidis, M. G. *J. Am. Chem. Soc.* **1995**, *117*, 1294−1301.
(21) Evenson, C. R.; Dorhout, P. K. *Inorg. Chem.* **2001**, *40*, 2409−2414.
(22) Wilkinson, F.; Kelly, G. *CRC Handbook of Organic Photochemistry*, Vol. 1; Scaiano, J. C., Ed.; CRC Press: Boca Raton, FL, 1989; pp 293−314.

Table 2. Selected Interatomic Distances[a] for $KSmGeSe_4$, **I**

		$SmSe_7$	
Sm−Se(2)	2.952(3)	Sm−Se(1)	2.966(2)
Sm−Se(4)	2.991(3)	Sm−Se(4)	2.998(3)
Sm−Se(3)	3.029(3)	Sm−Se(3)	3.039(3)
Sm−Se(1)	3.112(2)		
		$GeSe_4$	
Ge−Se(2)	2.312(3)	Ge−Se(4)	2.348(3)
Ge−Se(1)	2.349(3)	Ge−Se(3)	2.351(3)
		KSe_8	
K−Se(1)	3.308(6)	K−Se(2)	3.386(5)
K−Se(3)	3.448(7)	K−Se(4)	3.465(6)
K−Se(2)	3.508(9)	K−Se(3)	3.521(6)
K−Se(4)	3.546(6)	K−Se(2)	3.858(9)

[a] Distances are given in angstroms.

racemic twinning observed in **I** is consistent with that observed in $KLaGeSe_4$.[14]

Selected interatomic distances in **I** are shown in Table 2. **I** shows the expected lanthanide contraction when its lanthanide environment is compared to that of its closest structural analogue, $KLaGeSe_4$.[14] La−Se bonds in $KLaGeSe_4$ were observed ranging between 3.050 and 3.210 Å, as compared to Sm−Se bonds in **I** of 2.952−3.112 Å. The germanium environments of these two structures are identical to 95% confidence, but the K−Se interatomic distances in **I** are 0.02 Å longer, on average, than K−Se distances in $KLaGeSe_4$. This may be understood by comparing the unit cells. The *a* and *b* cell dimensions (parallel to the layers) in **I** are smaller than the equivalent cell edges in $KLaGeSe_4$ by 0.101 and 0.008 Å, respectively, while the *c* cell edge (perpendicular to the layers) in **I** is larger than the equivalent edge in $KLaGeSe_4$ by 0.018 Å. Since potassium occupies interlayer sites and is the least interacting species, the expanded *c* axis results in longer K−Se interatomic distances. This effect is likely due to lattice expansion in $KSmGeSe_4$ at a higher data collection temperature (data for $KLaGeSe_4$ were collected at 115 K). Incidentally, the expansion of the *c* axis is inconsistent with the trend observed for $KLnGeS_4$ (Ln = La, Gd, Nd),[14] in which all of the unit cell axes decreased as the size of the lanthanide cation decreased, but lattice constants of all of the members of this series were measured at 115 K.

$RbSmGeSe_4$, II, and $CsSmGeSe_4$, III. A single crystal of $RbSmGeSe_4$, **II**, was selected, 7076 (1196 independent) reflections were collected, and an absorption correction was applied ($R_{int} = 0.0901$). Data were collected within a θ range of 3.12−23.25° to a completeness of 99.9% with a data index range of $-7 \le h \le 7$, $-7 \le k \le 7$, $-19 \le l \le 19$. The space group $P2_12_12_1$ was uniquely determined through systematic absence analysis. The structure was solved by direct methods with final electron density residuals of 0.980 and −1.021 e Å^{-3}, and all atoms were refined anisotropically on F^2 for 65 variables.[19] Data for the isostructural $CsSmGeSe_4$, **III**, were collected from a single crystal by use of 7399 (1251 independent) reflections with an empirical absorption correction ($R_{int} = 0.0984$). Data were collected within a θ range of 3.09−23.31° to a completeness of 99.5% with a data index range of $-7 \le h \le 7$, $-7 \le k \le 7$, $-20 \le l \le 20$. The structure was solved by direct methods with final electron density residuals of 0.992 and −1.497 e Å^{-3}, and all atoms were refined anisotropically on F^2 for 64 variables.[19] Fractional coordinates and isotropic displacement parameters for $RbSmGeSe_4$ and $CsSmGeSe_4$ can be found in the Supporting Information.

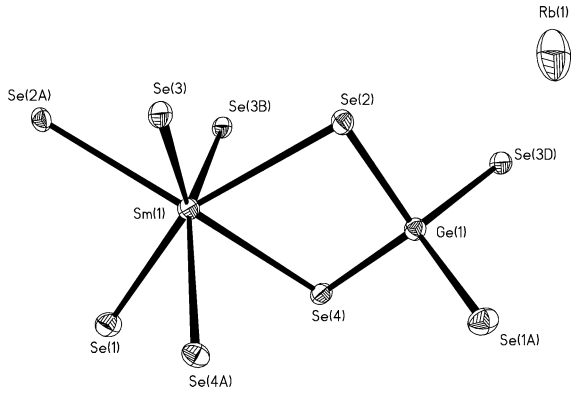

Figure 4. Thermal ellipsoid plot of $RbSmGeSe_4$ **II**, showing anisotropic displacement ellipsoids at 50% probability.

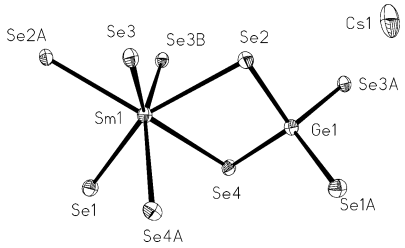

Figure 5. Thermal ellipsoid plot of $CsSmGeSe_4$ **III**, showing anisotropic displacement ellipsoids at 50% probability.

II and **III** are both isostructural with $CsSmGeS_4$,[13] first reported by Bucher and Hwu. This structure is shown viewed along the *a*-axis in Figure 1b and viewed along the *c*-axis in Figure 2b. Sm and Ge environments in **II** and **III**, as well as anisotropic displacement ellipsoids, are depicted in Figures 4 and 5, respectively. These layered structures consist of corner- and edge-sharing monocapped trigonal-prismatic $SmSe_7$ polyhedra, again corner- and edge-sharing with $GeSe_4$ tetrahedra, with Rb or Cs occupying the interlayer sites. The $SmSe_7$ polyhedra again form edge-sharing chains that run along the crystallographic *b*-axis, corner-sharing along the crystallographic *a*-axis, and tethered together with $GeSe_4$ tetrahedra as in **I**. As expected, the unit cell of **III** is swelled relative to **II** along the *c*-axis (perpendicular to the layers) due to the increased size of Cs relative to Rb. In **II** and **III**, the *c*-axis is doubled relative to that of **I** due to a 2_1 screw-axis relationship between bilayers of $SmGeSe_4$, whereas in **I**, each layer is identical in orientation.

Selected interatomic distances for **II** and **III** are displayed in Tables 3 and 4, respectively. When Sm−Se bond distances in **I**, **II**, and **III** are compared, the Sm environments are nearly identical. The average Sm−Se bond length in each of these compounds is 3.01 Å, with statistically insignificant variation. Similarly, the germanium environments in all three compounds are identical to within 95% confidence. Contrary to Bucher and Hwu,[13] we assert that Rb and Cs are each 11-coordinate, rather than 8-coordinate, each with a tripod of three long bonds extending along the +*a* crystallographic

Table 3. Selected Interatomic Distances[a] for $RbSmGeSe_4$, **II**

	$SmSe_7$		
Sm−Se(4)	2.953(2)	Sm−Se(1)	2.976(2)
Sm−Se(3)	2.986(2)	Sm−Se(3)	2.997(2)
Sm−Se(2)	3.021(2)	Sm−Se(2)	3.037(2)
Sm−Se(4)	3.107(2)		
	$GeSe_4$		
Ge−Se(1)	2.313(2)	Ge−Se(4)	2.348(3)
Ge−Se(3)	2.349(3)	Ge−Se(2)	2.353(3)
	$RbSe_{11}$		
Rb−Se(4)	3.364(3)	Rb−Se(1)	3.540(3)
Rb−Se(2)	3.582(3)	Rb−Se(1)	3.599(4)
Rb−Se(3)	3.700(3)	Rb−Se(1)	3.713(4)
Rb−Se(3)	3.757(3)	Rb−Se(2)	3.933(3)
Rb−Se(1)	4.325(3)	Rb−Se(2)	4.600(3)
Rb−Se(3)	4.839(3)		

[a] Distances are given in angstroms.

Table 4. Selected Interatomic Distances[a] for $CsSmGeSe_4$, **III**

	$SmSe_7$		
Sm−Se(4)	2.943(2)	Sm−Se(1)	2.978(2)
Sm−Se(3)	2.9836(2)	Sm−Se(3)	3.002(2)
Sm−Se(2)	3.023(2)	Sm−Se(2)	3.048(2)
Sm−Se(4)	3.121(2)		
	$GeSe_4$		
Ge−Se(1)	2.316(2)	Ge−Se(4)	2.347(2)
Ge−Se(3)	2.352(2)	Ge−Se(2)	2.355(2)
	$CsSe_{11}$		
Cs−Se(4)	3.498(2)	Cs−Se(1)	3.657(3)
Cs−Se(1)	3.685(2)	Cs−Se(2)	3.729(2)
Cs−Se(1)	3.755(3)	Cs−Se(3)	3.816(2)
Cs−Se(3)	3.901(2)	Cs−Se(2)	4.062(2)
Cs−Se(1)	4.326(2)	Cs−Se(2)	4.568(2)
Cs−Se(3)	4.817(2)		

[a] Distances are given in angstroms.

direction. Without these long bonds, Rb and Cs seem anomalously distorted within their environments toward the $-a$ direction. The 11-coordinate Rb sites in **II** result in Rb−Se interatomic distances of 3.4−4.6 Å, and Cs sites in **III** have Cs−Se interatomic distances of 3.5−4.6 Å. These interatomic distances are similar to those found in other alkali lanthanide selenides. For example, in the channel structure $CsEr_3Se_5$, Cs resides in a 9-coordinate tricapped trigonal-prismatic environment with interatomic distances 3.619−4.986 Å.[23]

$NaSmGeSe_4$, IV. The sodium analogue of the series presented a series of difficulties that has to date prevented complete structural analysis. The relatively low yield (less than 1%) and poor reproducibility of product formation, as compared to **I**−**III**, resulted in few crystals suitable for X-ray analysis. These crystals were quite small, and attempts to collect data on larger crystals revealed that the crystals were easily fractured perpendicular to the *b*-axis. **IV** is also metastable with other Sm-containing phases, including $NaSmSe_2$, and $Na_9Sm(Ge_2Se_6)_2$,[24] and experimental modification of the reaction stoichiometry failed to purify the desired phase.

A small triclinic unit cell [$a = 6.897(2)$ Å, $b = 9.919(2)$ Å, $c = 11.183(2)$ Å, $\alpha = 84.067(4)°$, $\beta = 88.105(4)°$, $\gamma = 73.999(4)°$, and $V = 731.5(3)$ Å^3] was repeatedly observed during the analysis of **IV**. To the authors' knowledge, this cell is not closely related to that of any published structure, and all attempts to generate higher symmetry unit cells failed. Two complete data sets have been collected on this compound, and in each resulting model electron density peaks consistent with distorted $GeSe_4$ tetrahedra were observed. Likewise, large electron density peaks consistent with Sm were found in 7- or 8-coordinate environments. Similar to the structures **I**−**III**, the Sm, Ge, and Se packed together in two-dimensional layers. However, the electron density between the layers was very diffuse and likely represents disorder in the sodium atom positions. In the model that generated the best fit to the data, one of these interlayer electron peaks was tentatively assigned as a fractionally occupied selenium bridge, related to the Se−Se unit observed in $K_2EuGeSe_5$.[25] Due to inherent problems associated with the assignment of atomic positions to disordered structures, this model is not presented here, but the unit cell is included for reference.

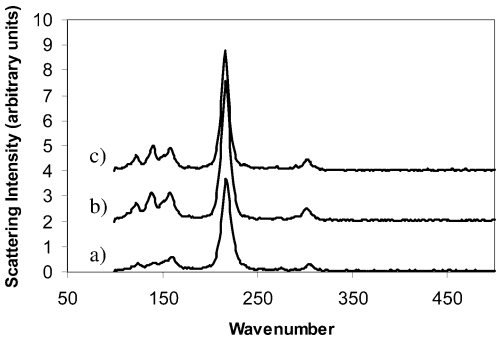

Figure 6. Raman spectra of $ASmGeSe_4$ compounds (a) $KSmGeSe_4$, (b) $RbSmGeSe_4$, and (c) $CsSmGeSe_4$.

Spectroscopic Analysis. Raman analysis of **I**−**III** in the region of 200 cm^{-1} provides information about the local environment of the germanium atoms in the structure (Figure 6). The structural similarities of the germanium environments in **I**−**III** is reflected in the nearly identical stretching and bending frequencies in Figure 6. Raman analysis of the corner-sharing $GeSe_4$ tetrahedra in $GeSe_2$ by Popovic[26] has shown that besides the primary symmetric stretch (A_1, 219 cm^{-1}), the Raman spectrum consists of two regions: bending modes (unassigned) < 150 cm^{-1}, and stretching modes from interconnected tetrahedra (T_2) between 250 and 340 cm^{-1}. These features are present in the spectra presented here with some minor differences. The similarity in the A_1 mode of the structures presented here, as compared to $GeSe_2$, shows that this vibrational mode is largely unaffected by the Sm and alkali inclusions.

Efforts were made to synthesize highly pure materials for this experiment, since impurities in the form of ternary alkali selenogermanates complicate the Raman spectra. After examining Raman spectra of several impure compounds we have realized that a previously published Raman spectrum of $KEuGeS_4$ (isostructural with $KSmGeSe_4$) likely contained

(23) Kim, S.-J.; Park, S.-J.; Yun, H.; Do, J. *Inorg. Chem.* **1996**, *35*, 5283−5289.
(24) Martin, B. R.; Polykova, L.; Dorhout, P. K. *Inorg. Chem.* (submitted for publication).
(25) Evenson, C. R.; Dorhout, P. K. *Inorg. Chem.* **2001**, *40*, 2409−2414.
(26) Popovic, Z. V. *Fizika* **1983**, *15*, 11−27.

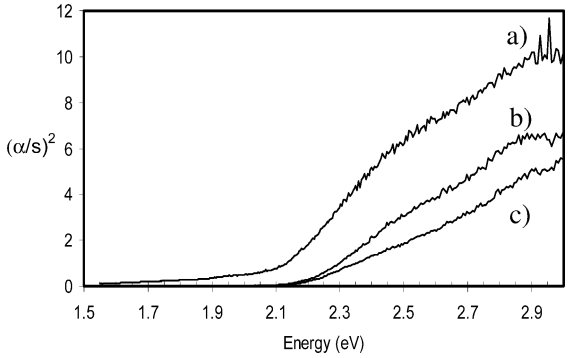

Figure 7. Diffuse reflectance spectra of (a) $RbSmGeSe_4$, **II**; (b) $KSmGeSe_4$, **I**; and (c) $CsSmGeSe_4$, **III**. Reflectance data have been converted to $(\alpha/s)^2$ by the Kubelka−Munk function.

impurities.[25] In this structure, the large A_1 peak at 380 cm^{-1} is probably correctly assigned, but the two peaks at 425 and 442 cm^{-1} are probably caused by thiogermanate impurities.

Analysis of diffuse reflectance UV−visible spectra of **I**−**III** revealed that all three structures have the same optical band gap of 2.2 eV, as extrapolated from the linear portion of the Kubelka−Munk corrected reflectance data (Figure 7). This measurement is consistent with the observed color (red-orange) of the crystals. The similarities of Sm environments in these structures lead to similar electronic structures, and the effect of layer stacking in these materials appears to be insignificant.

Discussion

Examination of the alkali metal environments in structures **I**−**III** reveals the fundamental differences between these structures, and these packing considerations are likely the driving force for their formation. K sites in **I** are in a bicapped trigonal prismatic 8-coordinate environment with K−Se interatomic distances of 3.3−3.9 Å. The rotation of alternate layers by 180° results in larger coordination environments around Rb and Cs in **II** and **III**. As the size of the alkali metal in the structures presented here increases, the unit cell expands to accommodate this cation. The expected increase in density in structures **I**−**III** is observed as the atomic mass of the alkali metal increases.

The $GeSe_4$ environments are quite similar in all the structures. In **I**, for example, Se−Ge−Se bond angles range from 100.8° to 115.6°. **II** and **III** have $GeSe_4$ environments with Se−Ge−Se bond angles of 102.0−111.7° and 102.6−111.5°, respectively. In all of these structures, $GeSe_4$ tetrahedra edge-share on three sides with $SmSe_7$ polyhedra. The $GeSe_4$ tetrahedra are therefore distorted with short bond angles on the shared edges.

Although $RbSmGeSe_4$ and $CsSmGeSe_4$ are isostructural, there is one significant difference between **II** and **III**. Both **II** and **III** were tested for racemic twinning, but the resulting absolute structure parameters were significantly different. Like $CsSmGeS_4$,[13] **III** was solved as a single enantiomorph, with an absolute structure parameter of 0.06(6). However, **II** showed significant racemic twinning, with an absolute structure parameter of 0.51(8). This effect could be explained by assuming that structure inversion occurs at the alkali metal layers. If strain is induced in the crystal by structure inversion, it is reasonable to assume that there must be some distortion in the alkali metal positions to accommodate this strain. Smaller alkali metal cations that fit loosely into their coordination environments could reorganize more effectively than large cations that fit tightly into well-defined cavities. Therefore, Rb allows structure inversion, while Cs does not. The similarity in A−Se interatomic distances in **II** and **III** despite the difference in ionic radii supports this proposal. In our hands, $CsSmGeSe_4$ was also obtained at a higher purity than $RbSmGeSe_4$ under similar reaction conditions, indicating that the Cs-containing quaternary product may be more stable, relative to ternary and binary byproducts, than the corresponding quaternary Rb product. Application of this logic to the $KSmGeSe_4$ structure type may yield a pure enantiomer in the $P2_1$ space group by use of a slightly larger cation in the alkali position.

As discussed by Wu and Ibers,[14] the $KLaGeSe_4$ structure-type is related to the Eu_2GeS_4 structure. This is especially interesting in light of the fact that Eu_2GeS_4 has been shown to be a ferroelectric material with a Curie transition temperature of 335 K.[27] A relaxation in the GeS_4 tetrahedra alters the coordination environment around one of the europium sites, resulting in a centrosymmetric $P2_1/m$ structure at high temperatures. This type of asymmetry is present in structures **I**−**III**, so it is reasonable to expect that these materials may also undergo a ferroelectric transition under the proper conditions. Studies of thermal- and pressure-induced transitions of these materials are underway.

Conclusions

Through the simple substitution of different alkali metals into a layered structure, the stacking behavior of samarium selenogermanate layers has been altered. Although the relationships between the structures of $CsSmGeS_4$ and $KLaGeSe_4$ have been noted previously, no deductions could be drawn concerning what might drive the formation of these separate phases, since the two compounds were synthesized under completely different conditions. The unit cell of the sodium analogue is included with the intention that this intriguing compound will spark further investigation into these materials.

This report is not designed to be a comprehensive study of all the possible structures involving the reactants described here. Rather, this paper is designed to point out the similarities between the related structures that formed and to emphasize the differences between them. Certain reaction systems exhibit more diversity in reaction products. In the Na−Sm−Ge−Se system, for example, another new structure type has been generated with a stoichiometry that is quite different from the structures in this report, $Na_9Sm(Ge_2Se_6)_2$.[24] It is unlikely that the other structures presented here represent unique quaternary phases for the component elements. Different reaction conditions may well favor the formation of different structures by locking the species into kinetically stabilized organizations. However, we believe that systematic

(27) Tampier, M.; Johrendt, D. *J. Solid State Chem.* **2001**, *158*, 343−348.

study of many structures generated from similar reaction conditions can yield valuable insight into the packing conditions that determine the final structure and will hopefully prove useful to those trying to systematically study the properties of solid-state structures.

Acknowledgment. Financial support was provided by the National Science Foundation, Grant CHE-0076180. We are also grateful to Dr. Agnete la Cour and Susie Miller for their help with crystallography. This work made use of the Electron Microscopy Center at the Colorado State University.

Supporting Information Available: Crystallographic data in CIF format. This material is available free of charge via the Internet at http://pubs.acs.org.

IC034724Y